FEIIC International Journal of Engineering and Technology

Research Article

Enhanced Lithium Recovery from Brines Using Titanium-Based Li_2TiO_3 Adsorbents Prepared via Sol-Gel Method

Kong Qianyu[1] and Nordin Sabli[1,2,*]

[1] Department of Chemical and Environmental Engineering, Faculty of Engineering, Universiti Putra Malaysia, 43400, UPM Serdang, Selangor, Malaysia

[2] Institute of Advance Technology (ITMA), Universiti Putra Malaysia, 43400, UPM Serdang, Selangor, Malaysia

*Corresponding author: nordin_sab@upm.edu.my

ABSTRACT

Li_2TiO_3 adsorbents were synthesized via a sol–gel method and evaluated for selective lithium-ion recovery from alkaline solutions. X-ray diffraction and Fourier-transform infrared spectroscopy confirmed the successful formation of crystalline Li_2TiO_3 with a TiO_6 octahedral structure. Acid leaching effectively removed lattice lithium, generating ion-exchange sites that enabled selective Li^+ adsorption through a memory effect mechanism. Grain size analysis based on XRD revealed crystallite growth from approximately 12.5 nm to 25.3 nm with increasing calcination temperature. Batch adsorption experiments demonstrated a maximum lithium-ion uptake of 16.2 $mg{\cdot}g^{-1}$ in 4 $g{\cdot}L^{-1}$ LiOH solution, with rapid adsorption equilibrium achieved within the initial adsorption period. Selectivity tests confirmed strong preferential adsorption of Li^+ over competing ions under alkaline conditions. Furthermore, the adsorbent retained approximately 84% of its initial adsorption capacity after five adsorption–desorption cycles, indicating good structural stability and reusability. The results demonstrate that sol–gel-derived Li_2TiO_3 offers a simple, stable, and effective route for selective lithium recovery from brine-type solutions.

Keywords. Lithium adsorption, titanium-based adsorbents, sol-gel synthesis, Li_2TiO_3 ion sieves, selective lithium recovery

1. INTRODUCTION

Lithium, a lightweight alkali metal, is increasingly recognized for its pivotal role in the global energy transition. Its high electrochemical reactivity and energy density have positioned it at the forefront of energy storage technologies, particularly in the production of lithium-ion batteries for electric vehicles, portable electronics, and grid-scale renewable energy systems [1-3]. The adoption of lithium-based systems has significantly reduced greenhouse gas emissions compared to conventional fossil-fuel technologies, making lithium a strategic material in the fight against climate change [4].

The global demand for lithium is accelerating rapidly, with projections indicating an annual growth rate of approximately 10%, effectively doubling consumption every decade [5]. This exponential growth, driven by industrialization and the rise of green technologies, has heightened the urgency for efficient and sustainable lithium extraction processes [6]. Lithium resources exist in both terrestrial and marine environments, including lithium-rich brines, ores, and seawater. While seawater holds immense theoretical reserves (~230 billion tonnes), salt lake brines offer more practical extraction routes due to higher lithium concentrations and simpler purification process [7-9].

Among the various extraction techniques, adsorption using lithium-ion sieves has emerged as a promising method due to its low cost, operational simplicity, and ion selectivity. Titanium-based sieves, particularly lithium titanate (Li_2TiO_3), have attracted significant attention for their chemical and thermal stability, as well as their ability to selectively capture lithium ions even in the presence of competing ions [10-11]. However, the performance of these adsorbents is strongly dependent on synthesis method employed.

Traditionally, solid-phase and hydrothermal methods have been used to synthesize Li_2TiO_3. While

effective, these techniques present several limitations: the solid-state method often suffers from incomplete reaction and poor particle dispersion, while the hydrothermal method requires high-pressure reactors and yields limited product quantities under harsh conditions. Furthermore, the solid-phase method demands a higher lithium-to-titanium molar ratio to compensate for lithium sublimation during high-temperature processing, leading to higher cost and material wastage [12].

In contrast, the sol-gel (SG) method has recently garnered interest as a more sustainable alternative for Li_2TiO_3 synthesis. The SG approach offers several advantages: it operates under milder conditions, enables homogeneous mixing at the molecular level, and allows precise control over particle size, morphology, and porosity. As demonstrated by recent studies, Li_2TiO_3 prepared via SG shows improved adsorption capacities (22–24 $mg \cdot g^{-1}$) under optimized pH conditions (typically pH 12), outperforming many solid-state syntheses with lower capacities (3–12 $mg \cdot g^{-1}$) and inferior recyclability. While hydrothermal synthesis may reach higher capacities (30 $mg \cdot g^{-1}$), it requires more energy-intensive and less scalable conditions. Moreover, SG-derived adsorbents show enhanced regeneration potential, which is critical for industrial reuse.

Despite these promising findings, the application of the SG method in Li_2TiO_3 synthesis remains underexplored. Key factors such as calcination temperature, solution pH, and lithium precursor type require further investigation to optimize material performance. Moreover, the influence of adsorption environment variables including lithium concentration, competing ions, and pH on adsorption and desorption behavior remains insufficiently characterized in existing literature.

Therefore, this study aims to systematically evaluate the sol-gel synthesis of Li_2TiO_3 and investigate the effects of synthesis parameters and operating conditions on the structural properties and lithium adsorption performance. The prepared materials are characterized using X-ray diffraction (XRD), Fourier-transform infrared spectroscopy (FTIR), and inductively coupled plasma (ICP) analysis to assess phase composition, functional group changes, and lithium uptake capacity. The regeneration ability and adsorption behavior under varying pH and ion concentrations are also examined to assess practical applicability. Ultimately, this work seeks to provide a simplified, scalable, and environmentally friendly approach to produce high-performance lithium adsorbents from Li_2TiO_3, contributing to the advancement of sustainable lithium recovery technologies for future energy systems.

2. MATERIALS AND METHODS

2.1. Chemicals and Reagents

All chemicals used in this study were of analytical grade and were utilized without further purification.

2.2. Instruments and Apparatus

The synthesis and characterization procedures employed a temperature-controlled magnetic stirrer (HJ-3), a blast drying oven (Model 101), and an electronic balance (FA2004N) for precise weighing.

2.3. Synthesis of Li_2TiO_3 Adsorbents

Li_2TiO_3 adsorbents were synthesized using a sol–gel (SG) method. Ethanol (C_2H_5OH) and deionized water were first mixed as the solvent system. Lithium acetate (CH_3COOLi) was dissolved in the mixed solvent to form solution A, while titanium butoxide ($Ti(OC_4H_9)_4$) was dissolved in ethanol with acetic acid as a stabilizing agent to form solution B. The two solutions were subsequently mixed at a lithium-to-titanium molar ratio of 2:1 under continuous stirring for 1 hr. The resulting sol was heated in a water bath at 60°C to promote gelation, followed by drying. The dried gel was then calcined in a muffle furnace at selected temperatures for 2 hr to obtain crystalline Li_2TiO_3 powders. After calcination, the powders were acid-washed using 0.25 M HCL to extract lattice lithium ions and generate H_2TiO_3 ion-sieve adsorbents. The acid-treated powders were filtered, thoroughly rinsed with deionized water until neutral pH was achieved and dried prior to adsorption experiments.

2.4. Reaction Mechanism

The synthesis process relies on the hydrolysis of titanium butoxide, resulting in the formation of $Ti(OH)_4$ intermediates. Acetic acid volatilization and carbon dioxide generation contribute to mass loss during heating [12].

2.5. Characterization

The crystal structure of the synthesized samples was analyzed using X-ray diffraction (XRD, Cu Kα radiation, λ = 1.54056 Å) over a 2θ range of 10–80° [13]. Fourier-transform infrared (FTIR) spectroscopy was performed using the KBr pellet method in the wavenumber range of 400–4,000 cm^{-1} to identify functional groups and structural changes before and after acid treatment [14]. Lithium ion concentrations in solution before and after adsorption were quantified using inductively coupled plasma optical emission spectrometry (ICP-OES) following appropriate dilution [15]. These characterization techniques were employed to evaluate phase composition, structural stability, and lithium adsorption performance.

3. RESULTS AND DISCUSSION

3.1. Characterization of Li_2TiO_3

Figure 1(a) presents the XRD patterns of Li_2TiO_3 (LTO) synthesized via the SG method and calcined at different temperatures for identical durations. It is evident that after a 2 hr treatment at 550°C, the Li_2TiO_3 crystalline phase is formed, characterized by relatively low and broad diffraction peaks. Upon increasing the temperature, a notable enhancement of the diffraction peaks is observed, along with a slight shift of each peak towards lower angles. At 750°C, the peaks further intensify. Consequently, it can be inferred that with increasing calcination temperatures, the diffraction peaks of Li_2TiO_3 become increasingly pronounced and sharper, indicating enhanced crystallinity and grain size enlargement. However, increasing the calcination temperature could trigger lithium sublimation during high-temperature treatment, resulting in a stepwise reduction of the lithium to titanium ratio in the final product. Such compositional change is likely to interfere with the Li^+ adsorption capability of the synthesized adsorbent. Hence, excessively high calcination temperatures should be avoided.

The crystallite size of Li_2TiO_3 was estimated using the Scherrer equation, $D=K\lambda/(\beta\cos\theta)$ [16], where K=0.89K = 0.89K=0.89, λ=1.54056 Å (Cu Kα), β is the full width at half maximum (FWHM), and θ is the Bragg angle of the main diffraction peak. For samples calcined at 550 °C, the main peak located at 2θ = 30.95° exhibited a FWHM of 0.398°, corresponding to a crystallite size of approximately 12.5 nm. When the calcination temperature was increased to 750 °C, the peak shifted slightly to 2θ = 30.88° with a reduced FWHM of 0.186°, yielding larger crystallite size of ~25.3 nm.

The results indicate that as the annealing temperature increases, the peak width (β) decreases, leading to an increase in the calculated grain size (D). This trend is consistent with grain growth behavior typically observed at higher temperatures. As the temperature rises from 550 °C to 750 °C, the peak width β of the Li2TiO3 main peak decreases from 0.398° to 0.186°, and the grain size D increases by about 2 times, from 12.5 nm to 25.3 nm. This indicates that increased temperature promotes grain growth.

As the temperature increases, the 2θ value of the main peak becomes smaller, and the d-value of the crystal plane increases from 2.917 Å to 2.946 Å. According to crystallographic principles, this is due to the thermal expansion effect caused by heating of the crystal lattice. The overall lattice expansion rate is about 1.0%. With increasing temperature, the relative intensity of the peaks decreases, and the intensity ratios change significantly. This may be because Li loss during heating, and new defect states are formed as TiO_2 precipitates out, resulting in changes in structure and composition.

3.2 XRD Patterns of Li_2TiO_3 Powders Under Various Conditions

Curve 1, 2, and 3 in Figure 1(b) represent the XRD curves of the adsorbent before pickling, after pickling, and after adsorption, respectively. Traditional titanium-based adsorbents are synthesized from titanium dioxide and lithium metatitanate, using conventional solid-state calcination to form lithium metatitanate [12,16]. The results demonstrate that all Li^+ ions can be extracted. In this experiment, Li_2TiO_3 was acid-washed for 8 hr. Figure 2 depicts the X-ray diffraction peaks of Li_2TiO_3 powders before and after acid washing, and post-lithium adsorption, illustrating the changes in the powders during acid washing and the reaction period.

Grain size calculation. The Scherrer formula was applied to estimate grain size [16]. From the XRD patterns, it can be seen that under various processing conditions, the main peak position and width of Li_2TiO_3 show no significant change, except that the main peak

intensity decreases slightly after acid washing. The absence of significant changes in peak width and peak position after acid washing and subsequent adsorption indicates that the crystallite size remains essentially unchanged within experimental uncertainty.

Peak shift detection. The 2θ value of the main peak shows no obvious shift after each processing step, and the corresponding d-spacing also remains basically unchanged. This demonstrates that there is no lattice expansion or contraction. The main diffraction peak of Li_2TiO_3 remained at approximately $2\theta \approx 30.9°$ before acid washing, after acid washing, and after lithium adsorption, indicating no measurable lattice expansion or contraction during these processes. Peak intensity variation. After acid washing, the relative intensity of the (–133) crystal plane reflection peak decreases markedly, implying partial removal of lattice Li^+ ions. Following lithium adsorption, partial recovery of the peak intensity is observed, suggesting re-embedding of lithium ions into available lattice or near-surface sites. These variations primarily reflect changes in lithium occupancy rather than alterations to Li_2TiO_3 crystal framework.

Overall, the XRD results demonstrate that the Li_2TiO_3 structure remains stable during acid washing and subsequent lithium adsorption. The ion-sieve behavior and memory-effect mechanism are therefore not inferred solely from XRD peak positions or intensities but are supported by previously reported studies on titanium-based lithium ion sieves [11,12,14], as well as recent literature describing lithium-selective ion-sieve mechanisms and reversible Li^+–H^+ exchange processes [17].

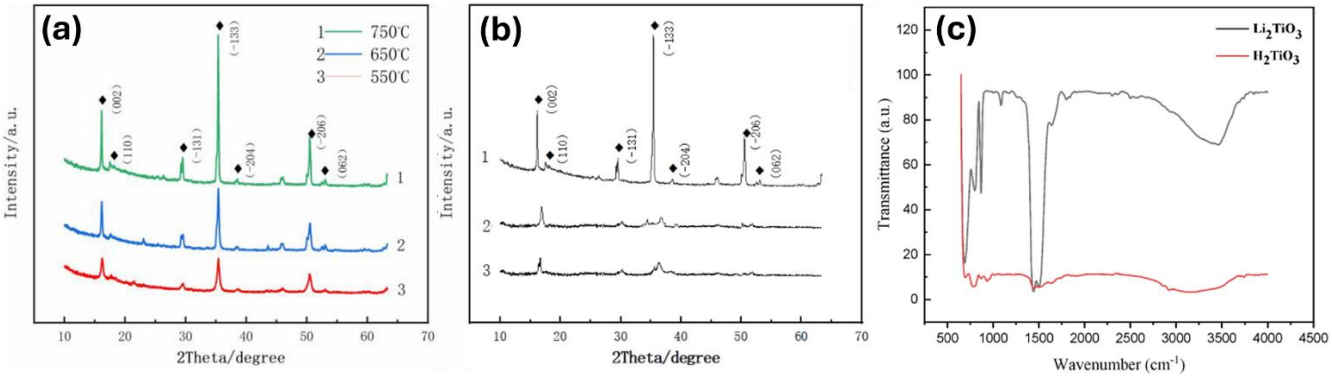

Figure 1. XRD patterns of (a) Li_2TiO_3 calcined at various temperatures (b) Li_2TiO_3 powders under various conditions and (c) FTIR spectroscopy patterns of Lithium Titanate (LTO)

Table 1. Adsorption capacity of adsorbents with different concentrations of LiOH solution

Time (hr)	Adsorption Capacity (mg.g^{-1})		
	0.5 g.L^{-1} LiOH	1.0 g.L^{-1} LiOH	4.0 g.L^{-1} LiOH
1.0	1.436	5.18	9.21
2.0	1.586	5.30	10.39
4.0	1.636	6.72	10.57
8.0	1.833	7.17	11.31
24.0	2.460	11.07	16.20

3.3. FTIR patterns of LTO

Figure 1(c) demonstrates Fourier Transform Infrared (FTIR) spectra of LTO and HTO synthesized at 650°C. The absorption bands observed in the low wavenumber region (approximately 400–900 cm^{-1}) are attributed to Ti–O stretching and Ti–O–Ti bending vibrations within the TiO_6 octahedral framework, which are characteristic of lithium titanate–based materials. For Li_2TiO_3, characteristic peaks in the low wavenumber region from 400 to 900 cm^{-1} correspond to the vibrations of metaloxygen bonds in the TiO_6 octahedral configuration, confirming its presence. The peaks

observed within the 1,000–1,650 cm^{-1} wavenumber regime can be majorly assigned to the characteristic vibrational modes of carbonate impurities. Additionally, broad bands approximating 3,000 cm^{-1} and 3,400 cm^{-1}, associated with O-H and N-H stretching vibrations, imply the presence of residual water and amino species in the examined sample.

For H_2TiO_3, the presence of the TiO_6 configuration is also detected in the 400-900 cm^{-1} region. However, unlike Li_2TiO_3, at 3,000 cm^{-1} and 3,400 cm^{-1} no significant O-H and N-H broad peaks are observed, indicating higher purity and fewer impurities in the H_2TiO_3 product. Both products successfully synthesized titanium oxalates with TiO_6 configurations. However, Li_2TiO_3 contained more carbonate and hydroxide impurities, likely due to side reactions during synthesis. To achieve purer products, further optimization of the synthesis conditions for Li_2TiO_3 is necessary.

3.4. Adsorption Performance Experiment

Table 1 outlines the residual lithium content and adsorption capacities using SG synthesized adsorbents in LiOH solutions of varying initial concentrations, denoted as LiOH(x) where x represents the starting LiOH amount in g^{-1}. Inductively coupled plasma atomic emission spectrometry quantified lithium quantities in the appropriately diluted solutions post-adsorption. Analyses unveil the highest and lowest adsorption efficiencies for LiOH(4.0) and LiOH(0.5) respectively, with LiOH(1.0) in between. At approximate 70% desorption, LiOH(4.0) excels, affirming that under specific concentration regimes, escalating initial lithium ion densities positively correlate with superior resultant uptake capacities.

3.4.1. Adsorption Capacity Over Time

Figure 2(a) depicts the lithium ion concentration in LiOH solutions of various concentrations using lithium titanate adsorbents synthesized via the SG method. The process was carried out under static conditions. The figure illustrates that the adsorption rate curves of the adsorbent at different concentrations follow a generally similar trend, indicating rapid adsorption. The highest adsorption rate occurs within the first hour, where up to 50% of the 24-hr adsorption capacity is achieved. Between 2 and 24 hr, the adsorption efficiency gradually levels off, and the adsorption capacity continues to increase with prolonged adsorption time.

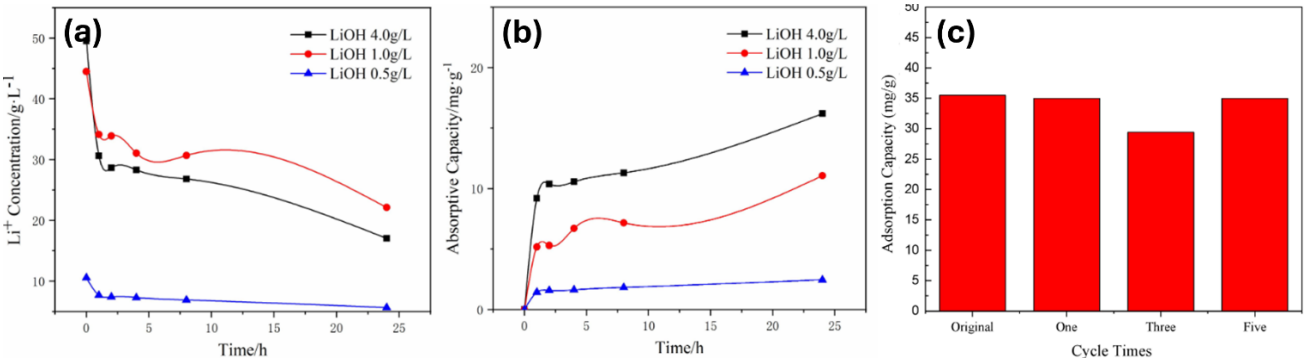

Figure 2. (a) Concentration of lithium ions measured in adsorption experiments with LiOH solution at different concentrations and for different times (b) Adsorption capacity of adsorbent in LiOH solutions of different concentrations (c) Cyclic adsorption performance of LTO adsorbents*[1].

Note*[1]: One", "three", and "five" denote representative adsorption–desorption cycles selected to illustrate the cycling performance of the adsorbent

Table 2. Adsorption results in LiOH solutions of different concentrations

Li^+ Initial Concentration ($g.L^{-1}$)	Adsorption Capacity ($mg.g^{-1}$)
0.5	2.46
1.0	11.07
4.0	16.20

3.4.2. Adsorption Capacity of Adsorbent at Different Concentrations

Figure 2(b) displays the adsorption capacity of Li^+ adsorbents prepared by the SG method. The figure reveals that the adsorption capacity rate is fastest within the first hour and positively correlates with the solution concentration. Between 2 and 24 hr, the adsorption capacity gradually increases at a decelerating pace. The adsorption capacity in a 4.0 $g{\cdot}L^{-1}$ LiOH solution is the highest, being twice that of the 1.0 $g{\cdot}L^{-1}$ LiOH solution and six times that of the 0.5 $g{\cdot}L^{-1}$ LiOH solution. The results signify that the adsorption capacity of the adsorbent material escalates markedly with the lithium ion concentration in the solution, and performs optimally within a certain elevated ionic concentration range. This can be attributable to two factors associated with increasing LiOH concentration. Firstly, the lithium ion quantity rises in the solution, thereby expedited capture onto adsorbent surfaces. Secondly, as dissolution of LiOH supplies abundant Li^+ that are continuously adsorbed onto adsorbents, proton release simultaneously occurs, facilitating ion exchange under alkaline conditions. The collective effects underscore the substantial role of LiOH content in governing the ultimate adsorption effectiveness

3.4.3. Adsorption in LiOH of Different Concentration

SG derived powders served as adsorbent precursors, using LiOH lithium sources at different concentrations and adsorption results are shown in Table 2. Sodium hydroxide addition tuned the pH to approximately 13, before conducting static adsorption tests. Upon attaining adsorption equilibrium, lithium ion residual levels were quantified to calculate uptake capacities as outline in Table 4. Evidently, escalations in initial lithium ion solution density simultaneously enhanced residual concentrations and equilibrium adsorption capacities. Results imply that lithium ion density negligibly influences adsorption kinetics at fixed pH conditions, whereas distinctly intensifying equilibrium adsorbent capacities. Therefore, superior lithium adsorption capacities accompany solutions with higher lithium content.

Table 3. Measurement table of selective adsorption experiment of lithium ion sieve

Time (hr)	Adsorption capacity ($mg.g^{-1}$)			
	0.5 $g.L^{-1}$ LiOH	1.0 $g.L^{-1}$ LiCl	0.5 $g.L^{-1}$ LiOH	1.0 $g.L^{-1}$ LiCl
1.0	1.436	5.18	1.496	5.09
2.0	1.586	5.30	1.548	5.12
4.0	1.636	6.72	1.732	6.98
8.0	1.833	7.17	1.890	7.53
24.0	2.460	11.07	2.543	10.87

3.5. Selective Adsorption Experiment

As shown in Table 3, at a constant lithium ion level and pH, the adsorption capacities obtained are roughly equal whether Lithium hydroxide and lithium chloride is used as the lithium source for adsorption. This indicates that the factors influencing the adsorption capacity are the lithium ion concentration and pH in the liquid, rather than the lithium source. The adsorbent exhibits selective absorptivity.

3.6. Cycling Performance Experiment

Figure 2(c) clearly demonstrates the lithium ion adsorption capacity of the material is able to maintain up to 84% of its initial capacity from the first cycle. “Original” refers to the adsorption capacity of the fresh adsorbent before cycling, while “one”, “two”, and subsequent labels correspond to the number of completed adsorption–desorption cycles. This indicates that the material possesses cyclic stability, suggesting its potential for repeated use in applications requiring lithium ion adsorption. This level of retention in adsorption capacity showcases the material's robustness against functional degradation over multiple cycles, making it a viable candidate for long-term usage in lithium ion recovery processes. Its ability to retain a significant portion of its initial

adsorption efficiency even after multiple cycles highlights its practical applicability in sustainable lithium ion extraction and recovery systems.

The lithium adsorption capacity obtained in this study (16.2 $mg \cdot g^{-1}$) is comparable to previously reported titanium-based lithium ion sieves derived from lithium titanate systems, which typically exhibit adsorption capacities in the range of approximately 10–30 $mg \cdot g^{-1}$ under alkaline conditions [11,12,14]. In addition, the observed capacity retention of 84% after five adsorption–desorption cycles is consistent with literature reports demonstrating stable cycling performance of Li_2TiO_3-based adsorbents [14,17]. These comparisons indicate that the present adsorbent exhibits representative and reliable lithium adsorption performance

4. CONCLUSIONS

This study has synthesized Li_2TiO_3 adsorbents through the SG technique and systematically evaluated their prospect as lithium ion adsorbents by structural characterization and performance analyses. The key conclusions are encapsulated below: XRD and FTIR analyses have shown that the crystal structure of the synthesized material conforms to the features of Li_2TiO_3 compounds, belonging to the TiO_6 octahedral configuration that constitutes a structural foundation beneficial for adsorption. Acid leaching results have indicated that lithium ions embedded within the lattice during synthesis could be effectively extracted in acid, leaving voids that demonstrate selective adsorption towards lithium ions. This establishes the basis for subsequent adsorption applications. The material has presented commendable adsorption capabilities towards lithium ions in solutions, achieving an adsorption capacity of 16.2 $mg \cdot g^{-1}$ in a 24h Li^+ solution and exhibiting rapid saturation kinetics across the entire adsorption process. This fully validates efficient adsorption performance. Selective adsorption tests have denoted that under analogous conditions, the material possesses approximate and highly efficient selective adsorption towards lithium ions across various sources, substantiating the specific adsorption traits. Cyclic adsorption trials have shown that after 5 continuous adsorption-desorption cycles, the material could retain 84% of its initial capacity, adequately proving its operational stability and durability while enabling efficient cyclic utilization.

5. ACKNOWLEDGEMENTS

The authors gratefully acknowledge the financial support provided by Akaun Amanah Master (6660800) for the Environmental Engineering Master Project.

6. REFERENCES

[1] Yasin, G., Arif, M., Mehtab, T., Lu, X., Yu, D., Muhammad, N., Nazir, M. T., & Song, H. (2020). Understanding and suppression strategies toward stable Li metal anode for safe lithium batteries. Energy Storage Materials, 25, 644–678. https://doi.org/10.1016/j.ensm.2019.09.020

[2] Nathan, A., Ahnood, A., Cole, M. T., Lee, S., Suzuki, Y., Hiralal, P., Bonaccorso, F., Hasan, T., Garcia-Gancedo, L., & others. (2012). Flexible electronics: the next ubiquitous platform. Proceedings of the IEEE, 100(Special Centennial Issue), 1486–1517. https://doi.org/10.1109/JPROC.2012.2190168

[3] Lochner, C. M., Khan, Y., Pierre, A., & Arias, A. C. (2014). All-organic optoelectronic sensor for pulse oximetry. Nature Communications, 5(1), 5745. https://doi.org/10.1038/ncomms6745

[4] Masias, A., Marcicki, J., & Paxton, W. A. (2021). Opportunities and Challenges of Lithium Ion Batteries in Automotive Applications. ACS Energy Letters, 6(2), 621–630. https://doi.org/10.1021/acsenergylett.0c02584

[5] Martin, G., Rentsch, L., Höck, M., & Bertau, M. (2017). Lithium market research - global supply, future demand and price development. Energy Storage Materials, 6, 171–179. https://doi.org/10.1016/j.ensm.2016.11.004

[6] Talens Peiró, L., Villalba Méndez, G., & Ayres, R. U. (2013). Lithium: Sources, Production, Uses, and Recovery Outlook. JOM, 65(8), 986–996. https://doi.org/10.1007/s11837-013-0666-4

[7] Bardi, U. (2010). Extracting Minerals from Seawater: An Energy Analysis. Sustainability, 2(4), Article 4. https://doi.org/10.3390/su2040980

[8] Murodjon, S., Yu, X., Li, M., Duo, J., Deng, T., & others. (2020). Lithium Recovery from Brines

Including Seawater, Salt Lake Brine, Underground Water and Geothermal Water. In Thermodynamics and Energy Engineering. https://doi.org/10.5772/intechopen.90371

[9] Speirs, J., Contestabile, M., Houari, Y., & Gross, R. (2014). The future of lithium availability for electric vehicle batteries. Renewable and Sustainable Energy Reviews, 35, 183–193. https://doi.org/10.1016/j.rser.2014.04.018

[10] Liu, C., Tao, B., Wang, Z., Wang, D., Guo, R., & Chen, L. (2021). Preparation and characterization of lithium ion sieves embedded in a hydroxyethyl cellulose cryogel for the continuous recovery of lithium from brine and seawater. Chemical Engineering Science. https://doi.org/10.1016/j.ces.2020.115984

[11] Wang, S., Zhang, M., Zhang, Y., Zhang, Y., Qiao, S., & Zheng, S. (2019). Application of citric acid as eluting medium for titanium type lithium ion sieve. Hydrometallurgy, 183, 166–174. https://doi.org/10.1016/j.hydromet.2018.12.002

[12] Tang, D., Zhou, D., Zhou, J., Zhang, P., Zhang, L., & Xia, Y. (2015). Preparation of H_2TiO_3–lithium adsorbent using low-grade titanium slag. Hydrometallurgy, 157, 90–96. https://doi.org/10.1016/j.hydromet.2015.07.009

[13] Zhou, Q., Oya, Y., Chikada, T., Zhang, W., Xue, L., & Yan, Y. (2017). Preparation of Li_2TiO_3 by hydrothermal synthesis and its structure evolution under high energy Ar^+ irradiation. Journal of the European Ceramic Society, 37(15), 4955–4961. https://doi.org/10.1016/j.jeurceramsoc.2017.06.032

[14] Liu, M., Wu, D., Qin, D., & Yang, G. (2022). Spray-drying assisted layer-structured H_2TiO_3 ion sieve synthesis and lithium adsorption performance. Chinese Journal of Chemical Engineering, 45, 258–267. https://doi.org/10.1016/j.cjche.2021.07.003

[15] Li, X., Chen, L., Chao, Y., Zhu, L., Luo, G., Sun, J., Jiang, L., Zhu, W., Liu, Z., & Xu, C. (2022). MXene Highly selective separation of lithium with hierarchical porous lithium-ion sieve microsphere derived from MXene. Desalination, 537, 115847. https://doi.org/10.1016/j.desal.2022.115847

[16] Zhang, L., Zhou, D., Yao, Q., & Zhou, J. (2016). Preparation of H_2TiO_3-lithium adsorbent by the sol–gel process and its adsorption performance. Applied Surface Science, 368, 82–87. https://doi.org/10.1016/j.apsusc.2016.01.203

[17] Ivanets, A., Bicheva, E., Prozorovich, V., Kouznetsova, T., Aimbetova, I. O., & Su, X. (2024). Effect of Ti-containing precursors on structure and adsorption performance of $Li_4Ti_5O_{12}$ and Li_2TiO_3 oxides to Li+ ions. Separation and Purification Technology, 335, 125986.